JCS ePress online publication date 24 January 2012

Research Article: MS# JOCES-2011-094185R1

Melanoregulin regulates retrograde melanosome transport through interaction with the RILP·p150^{Glued} complex in melanocytes

Norihiko Ohbayashi[1,‡], Yuto Maruta[1,‡], Morié Ishida[1] and Mitsunori Fukuda[1,§]

[1]Laboratory of Membrane Trafficking Mechanisms, Department of Developmental Biology and Neurosciences, Graduate School of Life Sciences, Tohoku University, Aobayama, Aoba-ku, Sendai, Miyagi 980-8578, Japan

(Running title: Mreg and retrograde melanosome transport)

Total number of words in the manuscript, including figure legends: 6278

[‡]These authors contributed equally to this work.

[§]Author for correspondence (nori@m.tohoku.ac.jp)

Abstract

Melanoregulin (Mreg), a *dilute suppressor* gene product, has been implicated in the regulation of melanosome transport in mammalian epidermal melanocytes, because Mreg deficiency was found to restore peripheral melanosome distribution from perinuclear melanosome aggregation in Rab27A-deficient melanocytes. However, the function of Mreg in melanosome transport has remained unknown. Here we show that Mreg regulates microtubule-dependent retrograde melanosome transport through the dynein-dynactin motor complex. Mreg interacted with the C-terminal domain of RILP (Rab interacting lysosomal protein) and formed a complex with RILP and $p150^{Glued}$, a component of the dynein-dynactin motor complex, in cultured cells. Overexpression of Mreg, RILP, or both in normal melanocytes induced perinuclear melanosome aggregation, whereas knockdown of Mreg or functional disruption of the dynein-dynactin motor complex restored peripheral melanosome distribution in Rab27A-deficient melanocytes. These findings reveal a novel mechanism by which the dynein-dynactin motor complex recognizes Mreg on mature melanosomes through interaction with RILP and is involved in their centripetal movement.

Keywords: *dilute suppressor*, Rab27A, hypopigmentation, microtubule-dependent transport, dynein-dynactin complex.

Introduction

Melanosomes are specialized organelles that synthesize and store melanin pigments in pigment cells. Pigmentation of mammalian hair and skin requires proper formation and transport of melanosomes along with two cytoskeletons, microtubules and actin filaments. Unlike other organelles, melanosomes are exceptionally visible under a light microscope, and thus are considered a good model system for analyzing organelle formation and transport (Marks and Seabra, 2001; Raposo and Marks, 2007). Three movements by melanosomes are defined by their speed, direction, and location in the cell, i.e., fast anterograde movement on microtubules towards their plus-ends at the periphery, fast retrograde movement on microtubules towards their minus-ends at the cell center, and slow movement on actin filaments at the cell periphery (Wu et al., 1998).

During the past decade, a tripartite protein complex composed of small GTPase Rab27A, its specific effector Slac2-a (also called melanophilin), and an actin-based motor myosin Va, has been shown to mediate actin-based melanosome transport in mammalian epidermal melanocytes (Fukuda et al., 2002; Provance et al., 2002; Strom et al., 2002; Wu et al., 2002; Fukuda, 2005), and the Rab-myosin transport system now appears to be a fundamental mechanism of organelle transport in many cell types (Seabra and Coudrier, 2004; Akhmanova and Hammer, 2010). Disruption of the tripartite protein complex, e.g., deficiency of Rab27A, causes the pigmentary dilution in human Griscelli syndrome patients and the corresponding mouse model (Van Gele et al.,

2009, and references therein) as a result of melanosome clustering around the nucleus (i.e., defect in transfer of melanosomes from microtubules to actin filaments). Interestingly, the diluted coat color phenotype of *dilute* (myosin Va-deficient), *ashen* (Rab27A-deficient), and *leaden* (Slac2-a-deficient) mice was found to be restored by a second mutation in the *dsu* (*dilute suppressor*) locus in 1983 (Sweet, 1983; Moore et al., 1988). However, although the *dsu* gene product, melanoregulin (Mreg; also called Dsu) (O'Sullivan et al., 2004; Boesze-Battaglia et al., 2007), has been implicated in the regulation of microtubule-dependent melanosome transport (Marks and Seabra, 2001), whose molecular machinery also remains to be elucidated in mammalian epidermal melanocytes, the function of Mreg in melanosome transport has remained unsolved for more than 25 years.

In this study we investigated the involvement of Mreg in the dynein-dynactin motor complex-dependent retrograde melanosome transport in melanocytes. We showed that Mreg forms a complex with RILP (Rab interacting lysosomal protein) and $p150^{Glued}$, a component of the dynein-dynactin motor complex. A possible function of Mreg as a cargo receptor for the dynein-dynactin motor complex is discussed based on our findings.

Results

Involvement of Mreg in microtubule-dependent retrograde melanosome transport. To investigate the possible role of Mreg in microtubule-dependent melanosome transport, we first overexpressed EGFP (enhanced green fluorescent protein)-tagged Mreg protein in black-mouse-derived melan-a cells (Bennett et al., 1987). As shown in Fig. 1A, EGFP-Mreg was clearly targeted to mature melanosomes (arrows in the inset of Fig. 1A; see also Fig. 2; endogenous Mreg is localized on mature melanosomes), and approximately 50% of the Mreg-expressing cells exhibited the perinuclear melanosome aggregation phenotype (Fig. 1E). Although Damek-Poprawa and co-workers have previously reported that Mreg-EGFP was localized at late endosomes/lysosomes, but not at mature melanosomes, in melanocytes (Damek-Poprawa et al., 2009), this discrepancy may be attributable to the use of different Mreg constructs, i.e., EGFP-Mreg (N-terminal EGFP-tag in this study) and Mreg-EGFP (C-terminal EGFP-tag in the previous study), suggesting that C-terminal EGFP-tagging may prevent the melanosomal localization of Mreg. To confirm the melanosomal localization of endogenous Mreg protein, mature melanosomes were affinity-purified using anti-Rab27A IgG and the presence of Mreg in the melanosomal fractions was investigated by immunoblotting. As expected, Mreg was clearly co-purified with three melanosome markers, Rab27A, tyrosinase, and Tyrp1, but was not co-purified with other organelle markers (Fig. 2).

Although consistent with a previous report on Mreg null mutant mice (Moore et

al., 1988) knockdown of endogenous Mreg in melan-a cells with specific shRNA had no effect on peripheral melanosome distribution (Fig. 1B, D(a), F), the same shRNA was able to re-disperse melanosomes to the cell periphery in Rab27A-defective melan-ash cells (Ali et al., 2004), which normally exhibit melanosome clustering around the nucleus (Bahadoran et al., 2001; Hume et al., 2001) (Fig. 1C, D(b), G, and Supplemental Fig. S1). It was evident, however, that the melanosomes in the Mreg-deficient melan-ash cells were not attached to the plasma membrane (Fig. 1C, insets in the middle two panels) because of a defect in the Rab27A·Slp2-a complex that is required for melanosome anchoring to the plasma membrane (Kuroda and Fukuda, 2004), in contrast to normal melan-a cells and Rab27A-re-expressing melan-ash cells, whose peripheral melanosomes were often observed just beneath the plasma membrane (Fig. 1C, inset in the far right panel).

The above results prompted us to hypothesize that Mreg is involved in the regulation of microtubule-dependent retrograde melanosome transport, and to test our hypothesis we investigated the involvement of a dynein-dynactin motor complex in the melanosome aggregation phenotype in melan-ash cells. As expected, disruption of the dynein-dynactin motor complex either by expression of $p50^{dynamitin}$, a negative regulator of dynein function (Burkhardt et al., 1997), or knockdown of $p150^{Glued}$, a subunit of dynactin, in melan-ash cells, phenocopied Mreg-deficient melan-ash cells (i.e., re-dispersion of melanosomes to the cell periphery) (Fig. 3A, B, D, E, and G). It should be noted that the Mreg-induced perinuclear melanosome aggregation phenotype in melan-a cells was almost completely eliminated by co-expression with $p50^{dynamitin}$ (Fig.

3C, F), strongly suggesting that Mreg is involved in retrograde melanosome transport through regulation of the dynein-dynactin motor complex.

Mreg forms a complex with RILP and p150^{Glued} both *in vitro* and in melanocytes. The results of a biochemical screening for the Mreg-binding partner in the dynein-dynactin motor complex or among its associated proteins by co-expression assay in COS-7 cells indicated that RILP (Fig. 4A), one of the p150^{Glued}-binding proteins involved in lysosomal transport to the cell center (Cantalupo et al., 2001; Jordens et al., 2001), interacted with Mreg (lane 7 in the middle panel of Fig. 4B). Interestingly, Mreg was unable to interact with RILP-L1, a close homologue of RILP (Wang et al., 2004) (Fig. 4A, and lane 8 in the middle panel of Fig. 4B). Consistent with these findings, knockdown of endogenous RILP, but not of RILP-Ll, in melan-ash cells also phenocopied Mreg-deficient melan-ash cells (Fig. 4C, D, E and Supplemental Fig. S2), but the same *RILP* shRNA had no effect on the peripheral melanosome distribution in melan-a cells, the same as the *Mreg* shRNA had no effect (Supplemental Fig. S2D).

Deletion analysis of RILP indicated that Mreg binds the C-terminal half of RILP (named RILP-C), which contains a second coiled-coil domain (CC2) (lane 3 in the top panel of Fig. 4F). We also attempted to determine the RILP-binding site in Mreg and prepared two deletion constructs, ΔN and ΔC (Fig. 5A). Interestingly, we found that RILP binds the C-terminal portion of Mreg (ΔN; Fig. 5B, lane 3), although the C-terminal portion of Mreg is not involved in melanosomal localization (Fig. 5C, middle panels). By contrast, the N-terminal portion of Mreg (ΔC; Fig. 5C, bottom

panels) was sufficient to show melanosomal localization, although this portion lacked RILP binding activity (Fig. 5B, lane 4).

Since RILP was originally described as a Rab7 effector (lane 3 in the middle panel of Fig. 4B) and the C-terminal half of RILP is responsible for Rab7 binding activity (Cantalupo et al., 2001; Wu et al., 2005), we proceeded to explore the relationship between Rab7-binding and Mreg-binding of RILP *in vitro*. A competition assay indicated that Rab7 and Mreg compete with each other for RILP binding (i.e., Mreg binding to RILP was clearly suppressed in the presence of an increasing amount of Rab7; compare the top and second panels in Fig. 4G), indicating that Mreg occupies the same or overlapping binding site as Rab7, which does not allow simultaneous binding. We did not directly compare the affinity of the RILP-Rab7 interaction with that of the RILP-Mreg interaction, but, as judged from the intensity of the bands in Fig. 4B, Rab7 seemed to bind RILP preferentially (compare lanes 3 and 7 in the middle panel).

Although Rab7 has been shown to function as a RILP·p150^{Glued} receptor in lysosomal transport (Jordens et al., 2001), based on the following observations Rab7 itself is unlikely to function in the process of retrograde melanosome transport. First, Rab7 is not present on mature melanosomes (insets in Supplemental Fig. S3A) and has already been shown to be involved in the transport of “early stage” melanosomes and not of mature melanosomes in primary human melanocytes (Jordens et al., 2006). Second, in contrast to Mreg overexpression, overexpression of a dominant active Rab7 mutant (i.e., Rab7(Q67L)) in melan-a cells had no effect on melanosome distribution (Supplemental Fig. S3A). Third, RNAi-mediated knockdown of Rab7 in melan-ash

cells failed to restore peripheral melanosome distribution (Supplemental Fig. S3B, C, D). To determine whether Mreg functions as a melanosomal receptor for RILP·p150^{Glued} in the retrograde transport of mature melanosomes by analogy to the function of Rab7 as a receptor for RILP·p150^{Glued} in lysosomal transport, we performed *in vitro* binding experiments using purified components (see Materials and Methods for details). As shown in Fig. 5D, Mreg formed a complex with purified RILP and p150^{Glued} (lane 2 in the top panel) and Mreg alone did not directly interact with p150^{Glued} (lane 1 in the top panel). Furthermore, the results of the co-immunoprecipitation assays using anti-Mreg-specific antibody indicated that endogenous Mreg is actually associated with p150^{Glued} in cultured melanocytes (lane 4 in the second panel of Figure 5E, and Supplemental Fig. S4). The association between Mreg and p150^{Glued} is likely to be RILP-dependent, because the knockdown of endogenous RILP causes a reduction in the amount of p150^{Glued} that is associated with Mreg (compare lanes 4 and 5/6 in the second and third panels of Fig. 5E).

Mreg functions as a RILP·p150^{Glued} receptor for retrograde melanosome transport. If Mreg actually functions as a RILP·p150^{Glued} receptor, expression of the Mreg-binding site of RILP (i.e., RILP-C) in melan-ash cells should cause re-dispersion of the melanosomes by disrupting the endogenous Mreg-RILP interaction (i.e., a dominant negative effect). As expected, monomeric strawberry (mStr)-tagged RILP-C was well targeted to mature melanosomes in melan-ash cells (arrows, upper inset in the bottom right panel of Fig. 6A), and its expression resulted in re-dispersion of the melanosomes

to the cell periphery, the same as Mreg knockdown in melan-ash cells did (Fig. 6A, B). By contrast, mStr-RILP-N was mostly present in the cytosol and did not rescue the perinuclear melanosome aggregation phenotype in melan-ash cells (Fig. 6A, B). Moreover, co-expression of mStr-RILP-C with EGFP-Mreg in melan-a cells also rescued the perinuclear melanosome aggregation phenotype induced by EGFP-Mreg (Fig. 6C, D), whereas expression of mStr-RILP-C alone in melan-a cells had no effect on peripheral melanosome distribution (Supplemental Fig. S5). By contrast, mStr-RILP-N again had no effect on melanosome distribution in control melan-a cells or EGFP-Mreg-expressing melan-a cells (Figs. 6C, D, and Supplemental Fig. S5). In contrast to the truncated RILP mutants, co-expression of full-length RILP with EGFP-Mreg in melan-a cells further increased the proportion of melanocytes showing perinuclear melanosome aggregation to approximately 80%, a much greater proportion than induced by solo expression of mStr-RILP-full or EGFP-Mreg (approximately 40%) (Fig. 6C, D).

Discussion

In the present study we have identified RILP as a novel binding partner of Mreg on mature melanosomes and demonstrated that Mreg is associated with the dynein-dynactin motor complex through interaction with RILP, a $p150^{Glued}$-binding partner (Fig. 4). *In vitro* binding experiments using purified components indicated that Mreg is able to directly interact with RILP (Fig. 5D). However, since the *in vitro* interaction between Mreg and RILP appeared to be weak, we cannot completely rule out the possibility that an additional unidentified factor may stabilize the Mreg-RILP-$p150^{Glued}$ interaction in melanocytes. RNAi-mediated knockdown of Mreg, RILP, or $p150^{Glued}$ (or overexpression of $p50^{dynamitin}$) in melan-ash cells resulted in the same melanosome dispersion phenotype (Figs. 1, 3, and 4C). This phenomenon is not a unique event in melan-ash cells, because the knockdown of Mreg, RILP, or $p150^{Glued}$ in cytochalasin D-treated melan-a cells also caused melanosomes to disperse from around the nucleus to the cell periphery (Supplemental Fig. S6). Conversely, expression of both Mreg and RILP in melan-a cells strongly induced perinuclear aggregation of melanosomes (Fig. 6). These results allowed us to conclude that the Mreg on mature melanosomes (i.e., lysosome-related organelles (Marks and Seabra, 2001; Blott and Griffiths, 2002)) recruits the dynein-dynactin motor complex through RILP, which is analogous to the recruitment of the dynein-dynactin motor complex to lysosomes (or secretory lysosomes) via Rab7 (Jordens et al., 2001; Johansson et al., 2007; Daniele et al., 2011) (a schematic model is shown in Supplemental Fig. S7). In contrast to our

finding that the knockdown of Mreg in melan-ash cells restores the peripheral melanosome distribution (Fig. 1C), however, O'Sullivan et al. (2004) previously reported that *dsu*/*dilute* double mutant did not reverse the *dilute* phenotype of perinuclear melanosome aggregation. This discrepancy may be reconciled by the presence of an alternative compensatory machinery. An additional dynein-dynactin cargo receptor other than Mreg may be present on mature melanosomes. Future extensive study will be necessary to address this issue.

Since both Mreg and RILP are expressed in a variety of mammalian tissues in addition to melanocytes (O'Sullivan et al., 2004; Wang et al., 2004; Damek-Poprawa et al., 2009), they may also be involved in the retrograde transport of Mreg-containing organelles to the cell center in other cell types. Interestingly, it has recently been reported that lysosome-dependent phagosome degradation activity is diminished in the retinal pigment epithelial cells of Mreg knockout mice (Damek-Poprawa et al., 2009). If Mreg is present on cathepsin D transport vesicles or engulfed materials in retinal pigment epithelial cells, this phenotype may be explained by inefficient retrograde transport of the vesicles to the cell center, where lysosomes are usually abundant. Further work is needed to determine whether Mreg actually functions as a cargo receptor for RILP·p150^{Glued} in retrograde transport in other cell types, including retinal pigment epithelial cells.

In conclusion, this study is the first to demonstrate that Mreg regulates microtubule-dependent retrograde melanosome transport through regulation of the dynein-dynactin motor complex likely as a cargo receptor on mature melanosomes.

Therefore, functional loss of Mreg in melan-ash cells caused re-distribution of melanosomes from the perinucleus to the cell periphery by suppression of retrograde melanosome transport.

Materials and Methods

Antibodies. The following antibodies used in this study were obtained commercially: anti-actin goat polyclonal antibody and horseradish peroxidase (HRP)-conjugated anti-GST antibody (Santa Cruz Biotechnology, Santa Cruz, CA, USA); anit-calreticulin rabbit polyclonal antibody (Thermo-Fisher Scientific, Waltham, MA, USA); anti-EEA1 (early endosomal antigen-1) rabbit monoclonal antibody (Cell signaling technology, Beverly, MA, USA); anti-EGFR (epidermal growth factor receptor) sheep polyclonal antibody (Fitzgerald Industries International, Concord, MA, USA); anti-GM130 mouse monoclonal antibody, anti-γ-adaptin mouse monoclonal antibody, anti-Lamp1 (lysosomal-associated membrane protein 1) rat monoclonal antibody (1D4b), and anti-p150^{Glued} mouse monoclonal antibody (BD Biosciences, Bedford, MA, USA); anti-Lamp1 rabbit polyclonal antibody (Abcam, Cambridge, UK); anti-Pmel17 mouse monoclonal antibody (HMB45; Dako, Carpinteria, CA, USA); anti-TfR (transferrin receptor) mouse monoclonal antibody (Invitrogen Corp., Carlsbad, CA, USA); anti-Tyrp1 (tyrosinase-related protein 1) mouse monoclonal antibody (Ta99; ID Labs, London, ON, Canada); anti-GFP (green fluorescent protein) rabbit polyclonal antibody (MBL, Nagoya, Japan); and HRP-conjugated anti-T7 tag mouse monoclonal antibody (Merck Biosciences Novagen, Darmstadt, Germany). Anti-tyrosinase rabbit polyclonal antibody and anti-Rab27A rabbit polyclonal antibody were prepared as described previously (Saegusa et al., 2006; Beaumont et al., 2011). Anti-FLAG rabbit polyclonal antibody, HRP-conjugated anti-FLAG tag (M2) mouse monoclonal antibody,

and anti-FLAG tag antibody-conjugated agaroase were obtained from Sigma-Aldrich Corp. (St. Louis, MO, USA).

GST-Mreg, GST-RILP-N (amino acids 1-199), and GST-Rab7 were expressed in bacteria and purified by standard protocols as described previously (Kuroda and Fukuda, 2005). Japanese White rabbits were immunized with the purified GST-Mreg (GST-RILP-N or GST-Rab7), and specific antibodies were affinity-purified by exposure to antigen-bound Affi-Gel 10 beads (Bio-Rad Laboratories, Hercules, CA, USA) according to the manufacturer's instructions (Fukuda and Mikoshiba, 1999).

Plasmid construction. cDNAs encoding the open reading frame of the mouse Mreg, RILP, $p50^{dynamitin}$, and $p150^{Glued}$ were amplified from Marathon-Ready adult mouse brain, liver, and/or testis cDNA (BD Biosciences Clontech, Mountain View, CA, USA) by PCR with specific pairs of oligonucleotides as described previously (Fukuda et al., 1999). Truncated mutants of RILP (i.e., RILP-N, amino acids 1-199; and RILP-C, amino acids 200-369; see Fig. 4F) and of Mreg (i.e., Mreg-ΔN, amino acids 76-214; and Mreg-ΔC, amino acids 1-139; see Fig. 5A) were also prepared by conventional PCR techniques. The oligonucleotide sequences used in this study are available from the authors on request. The cDNA fragments amplified were subcloned into the pEGFP-C1 vector (BD Biosciences Clontech), pmStr-C1 vector, which was obtained by replacing the EGFP insert of pEGFP-C1 with mStr, pEF-T7/T7-GST/FLAG/HA vectors (Fukuda et al., 1999), and/or pGEX-4T-3 vector (GE Healthcare Ltd., Little Chalfont, UK). pSilencer 2.1-U6 neo vector was from Ambion (Austin, TX, USA). pSilencer-Mreg-st1

(#1) (19-base target site: 5'-CTGCACTGCCTTCCATTTC-3'), pSilencer-Mreg-st2 (#2) (19-base target site: 5'-TCCGTATTCCTCCTTTGGA-3'), pSilencer-RILP-st1 (#1) (19-base target site: 5'-CAGAGCTTGGAACCTGATG-3'), pSilencer-RILP-st2 (#2) (19-base target site: 5'-GTCCAAGGTGTTTCTGCTG-3'), pSilencer-RILP-L1-st1 (#1) (19-base target site: 5'-GAATGAGGACGTCGAGGCT-3'), pSilencer-RILP-L1-st2 (#2) (19-base target site: 5'-GGAGGTGGTGGACAAGCAG-3'), pSilencer-Rab7-st1 (#1) (19-base target site: 5'-TTCCCTGAACCCATCAAAC-3'), and pSilencer-Rab7-st2 (#2) (19-base target site: 5'-GAAAGTGTTGCTGAAGGTC-3') were constructed essentially as described previously (Kuroda and Fukuda, 2004). Stealth RNA oligonucleotides against mouse $p150^{Glued}$ was obtained from Invitrogen Corp. (catalogue numbers MSS203510 and MSS203511; designated as #1 and #2, respectively). Since similar results were obtained with two independent shRNAs/siRNAs against Mreg, RILP, RILP-L1, $p150^{Glued}$, or Rab7, the effect of the siRNAs/shRNAs reported in this study must not be an off-target effect. pEGFP-C1-$Mreg^{SR}$ and pEGFP-C-1-$RILP^{SR}$ (siRNA-resistant mutants) were prepared by two-step PCR techniques as described previously (Tamura et al., 2011). Other expression plasmids, including pEF-FLAG-Rab7, pEF-FLAG-Rab27A, pEF-FLAG-Rab34, pEGFP-C1-Rab7, pEGFP-C1-Rab7(Q67L), and pEF-FLAG-RILP-L1, were prepared as described previously (Fukuda, 2003; Tsuboi and Fukuda, 2006; Fukuda et al., 2008).

Immunofluorescence analysis and melanosome distribution assay. The immortal

mouse melanocyte cell lines melan-a, derived from a black mouse, and melan-ash, derived from an *ashen* mouse (generous gift of Dorothy C. Bennett, St George's Hospital Medical School, London, UK), were cultured on glass-bottom dishes (35 mm dish; MatTek, Ashland, MA, USA) as described previously (Bennett et al., 1987; Kuroda et al., 2003; Ali et al., 2004). B16-F1 cells were also cultured as described previously (Kuroda et al., 2002). Plasmids (e.g., pmStr, pEGFP, and pSilencer vectors) were transfected into melanocytes by using FuGENE 6 (Roche Applied Science, Mannheim, Germany) according to the manufacturer's instructions. Two days after transfection, cells were fixed in 4% paraformaldehyde, permeabilized with 0.3% Triton X-100, and stained with the following antibodies: anti-p150^{Glued} mouse monoclonal antibody (1/100 dilution), anti-Mreg rabbit antibody (18.7 μg/ml), anti-FLAG rabbit polyclonal antibody (1/100 dilution), and anti-T7 tag mouse monoclonal antibody (1/300 dilution). The antibodies were visualized with anti-mouse/rabbit Alexa Fluor 488/594-conjugated IgG (Invitrogen Corp.), and examined for fluorescence with a confocal fluorescence microscope (Fluoview; Olympus, Tokyo, Japan). The images were processed with Adobe Photoshop software (CS3). Melanosome distribution assays (i.e., perinuclear aggregation versus peripheral dispersion) were performed as described previously (n >50 from three independent dishes) (Kuroda et al., 2003), and data are expressed as means and SD. Statistical analyses were performed by Student's unpaired *t* test.

Reverse transcriptase (RT)-PCR analysis. The total RNA of mouse melan-a cells (or

melan-ash cells) that had been transfected with pSilencer vectors twice was prepared using TRI-reagent (Sigma-Aldrich Corp.) and was subjected to reverse transcription using ReverTra Ace (Toyobo, Osaka, Japan) according to the manufacture's instructions. The cDNA of mouse Mreg, RILP, or RILP-L1 was amplified by PCR with the following pairs of oligonucleotides: 5'-GGATCCAATTTATGGAGCATGCCT-3' (Mreg-5' primer, sense) and 5'-GTCGACCATTTGGCTAGCAATCTT-3' (Mreg-3' primer, antisense) for Mreg; 5'-TCCAGAAGCTGTCCAGTGTG-3' (RILP-5' primer, sense) and 5'-TTGCTGTGGGGTCTCTTCTC-3' (RILP-3' primer, antisense) for RILP; and 5'-GGATCCATGGAGGAGCCGCTAGGGTC-3' (RILP-L1-5' primer, sense) and 5'-GTCGACCTCCTCCTCCCCATT-3' (RILP-L1-3' primer, antisense) for RILP-L1. The mouse G3PDH (glyceraldehyde 3-phosphate dehydrogenase) was amplified using mouse G3PDH-5' and G3PDH-3' primers (BD Biosciences Clontech) as a reference.

Immunoaffinity purification of mature melanosomes. Immunoaffinity purification of Rab27A-bound melanosomes with anti-Rab27A IgG-conjugated magnetic beads was also performed as described previously (Kuroda and Fukuda, 2004). In brief, B16-F1 cells (one confluent 10-cm dish) were homogenized in a homogenization buffer (5 mM HEPES-KOH, pH7.2, 5 mM EGTA, 0.03 M sucrose, and protease inhibitors (Complete; Roche Applied Science)). After centrifugation at 800 $\times g$ for 10 minutes, the supernatant obtained was incubated for 2 hours at 4°C with anti-Rab27A rabbit polyclonal antibody or control rabbit IgG in the presence of 1% BSA (bovine serum albumin), and then with Dynabeads M-280 (Invitrogen Corp.) for 30 minutes at 4°C. After washing the beads

twice with PBS (phosphate-buffered saline), the bound fractions were subjected to 10% SDS-PAGE followed by immunoblotting with the antibodies indicated in Fig. 2.

***In vitro* binding assays**. Co-immunoprecipitation assays in COS-7 cells (Figs. 4B and 5B) and GST pull-down assays (Fig. 4F) were performed as described previously (Fukuda et al., 1999; Fukuda and Kanno, 2005). In brief, T7-GST-RILP-N or T7-GST-RILP-C was transiently expressed in COS-7 cells and affinity-purified by glutathione-Sepharose beads (GE Healthcare Ltd.). Beads coupled with either T7-GST-RILP-N or T7-RILP-C were incubated for 2 hours at 4°C with COS-7 cell lysates containing HA-Mreg. After washing the beads three times with 1 ml of washing buffer (50 mM HEPES-KOH, pH7.2, 150 mM NaCl, and 1 mM $MgCl_2$), the proteins bound to the beads were analyzed by 10% SDS-PAGE followed by immunoblotting with HRP-conjugated anti-T7 tag antibody and anti-Mreg antibody. Similarly, FLAG-Mreg, FLAG-Mreg-ΔN, or FLAG-Mreg-ΔC was transiently expressed in COS-7 cells and affinity-purified by anti-FLAG tag antibody-conjugated agarose. Beads coupled with FLAG-Mreg truncated proteins were incubated for 2 hours at 4°C with COS-7 cell lysates containing T7-GST-RILP, and the proteins bound to the beads were analyzed by 10% SDS-PAGE followed by immunoblotting with HRP-conjugated anti-T7 tag antibody and HRP-conjugated anti-FLAG tag antibody.

Competition experiments between Mreg and Rab7 (Fig. 4G) was performed essentially as described previously (Fukuda et al., 2004). In brief, T7-GST-RILP-C1 was transiently expressed in COS-7 cells and affinity-purified by glutathione-Sepharose

beads. Beads coupled with T7-GST-RILP-C or beads alone were incubated for 2 hours at 4°C with COS-7 cell lysates containing T7-Mreg and/or increasing amount of FLAG-Rab7 in 50 mM HEPES-KOH, pH7.2, 150 mM NaCl, 1 mM $MgCl_2$, and 0.5 mM GTPγS. After washing the beads three times with 1 ml of the washing buffer, the proteins bound to the beads were analyzed by 10% SDS-PAGE followed by immunoblotting with anti-Mreg antibody, HRP-conjugated anti-FLAG tag antibody, and HRP-conjugated anti-T7 tag antibody.

For *in vitro* direct binding experiments, T7-GST-RILP and FLAG-$p150^{Glued}$ were transiently expressed in COS-7 cells and affinity-purified by glutathione-Sepharose beads and anti-FLAG tag-conjugated agarose beads, respectively, as described previously (Fukuda and Kanno, 2005). GST-Mreg was prepared from bacteria as described above. Beads coupled with FLAG-$p150^{Glued}$ were incubated for 2 hours with purified GST-Mreg alone or GST-Mreg and T7-GST-RILP in 50 mM HEPES-KOH, pH 7.2, 150 mM NaCl, 1 mM $MgCl_2$ and protease inhibitors (Complete; Roche Applied Science). After washing the beads three times with 1 ml of the washing buffer, the proteins bound to the beads were analyzed by 10% SDS-PAGE followed by immunoblotting with HRP-conjugated anti-GST antibody and HRP-conjugated anti-FLAG tag antibody.

Immunoprecipitation. Immunoprecipitation of the endogenous molecules from melanocyte lysates (Fig. 5E and Supplemental Fig. S4) were performed essentially as described previously (Fukuda and Kanno, 2005). In brief, the lysates from B16-F1 cells

transfected with pSilencer-RILP-st1/st2 (#1/#2) or pEF-FLAG-RILP were incubated for 2 hours at 4°C with either anti-Mreg rabbit polyclonal antibody described above or control rabbit IgG, and then with protein A-Sepharose beads for 1 hour at 4°C. After washing the beads three times with 1 ml of the washing buffer, the proteins bound to the beads were analyzed by 10% SDS-PAGE followed by immunoblotting with the indicated antibodies in Fig. 5E and Supplemental Fig. S4.

ACKNOWLEDGEMENTS

We thank Dr. Dorothy C. Bennett for kindly donating melan-a and melan-ash cells, Megumi Aizawa for technical assistance, and members of the Fukuda Laboratory for valuable discussions. This work was supported in part by Grants-in-Aid for Scientific Research from the Ministry of Education, Culture, Sports, and Technology (MEXT) of Japan (to N.O. and M.F.) and by a grant from the Global COE Program (Basic & Translational Research Center for Global Brain Science) of the MEXT of Japan (to N.O. and M.F.).

References

Akhmanova, A. and Hammer, J. A., III. (2010). Linking molecular motors to membrane cargo. *Curr. Opin. Cell Biol.* **22**, 479-487.

Ali, B. R., Wasmeier, C., Lamoreux, L., Strom, M. and Seabra, M. C. (2004). Multiple regions contribute to membrane targeting of Rab GTPases. *J. Cell Sci.* **117**, 6401-6412.

Bahadoran, P., Aberdam, E., Mantoux, F., Buscà, R., Bille, K., Yalman, N., de Saint-Basile, G., Casaroli-Marano, R., Ortonne, J. P. and Ballotti, R. (2001). Rab27a: a key to melanosome transport in human melanocytes. *J. Cell Biol.* **152**, 843-850.

Bennett, D. C., Cooper, P. J. and Hart, I. R. (1987). A line of non-tumorigenic mouse melanocytes, syngeneic with the B16 melanoma and requiring a tumour promoter for growth. *Int. J. Cancer* **39**, 414-418.

Beaumont, K. A., Hamilton, N. A., Moores, M. T., Brown, D. L., Ohbayashi, N., Cairncross, O., Cook, A. L., Smith, A. G., Misaki, R., Fukuda, M., Taguchi, T., Sturm, R. A. and Stow, J. L. (2011). The recycling endosome protein Rab17 regulates melanocytic filopodia formation and melanosome trafficking. *Traffic* **12**, 627-643.

Blott, E. J. and Griffiths, G. M. (2002). Secretory lysosomes. *Nat. Rev. Mol. Cell Biol.* **3**, 122-131.

Boesze-Battaglia, K., Song, H., Sokolov, M., Lillo, C., Pankoski-Walker, L.,

Gretzula, C., Gallagher, B., Rachel, R. A., Jenkins, N. A., Copeland, N. G. et al. (2007). The tetraspanin protein peripherin-2 forms a complex with melanoregulin, a putative membrane fusion regulator. *Biochemistry* **46**, 1256-1272.

Burkhardt, J. K., Echeverri, C. J., Nilsson, T. and Vallee, R. B. (1997). Overexpression of the dynamitin (p50) subunit of the dynactin complex disrupts dynein-dependent maintenance of membrane organelle distribution. *J. Cell Biol.* **139**, 469-484.

Cantalupo, G., Alifano, P., Roberti, V., Bruni, C. B. and Bucci, C. (2001). Rab-interacting lysosomal protein (RILP): the Rab7 effector required for transport to lysosomes. *EMBO J.* **20**, 683-693.

Damek-Poprawa, M., Diemer, T., Lopes, V. S., Lillo, C., Harper, D. C., Marks, M. S., Wu, Y., Sparrow, J. R., Rachel, R. A., Williams, D. S. et al. (2009). Melanoregulin (MREG) modulates lysosome function in pigment epithelial cells. *J. Biol. Chem.* **284**, 10877-10889.

Daniele, T., Hackmann, Y., Ritter, A. T., Wenham, M., Booth, S., Bossi, G., Schintler, M., Auer-Grumbach, M. and Griffiths, G. M. (2011). A role for Rab7 in the movement of secretory granules in cytotoxic T lymphocytes. *Traffic* **12**, 902-911.

Fukuda, M. (2003). Distinct Rab binding specificity of Rim1, Rim2, rabphilin, and Noc2: Identification of a critical determinant of Rab3A/Rab27A recognition by Rim2. *J. Biol. Chem.* **278**, 15373-15380.

Fukuda, M. (2005). Versatile role of Rab27 in membrane trafficking: focus on the Rab27 effector families. *J. Biochem.* **137**, 9-16.

Fukuda, M. and Mikoshiba, K. (1999). A novel alternatively spliced variant of synaptotagmin VI lacking a transmembrane domain: implications for distinct functions of the two isoforms. *J. Biol. Chem.* **274**, 31428-31434.

Fukuda, M. and Kanno, E. (2005). Analysis of the role of Rab27 effector Slp4-a/granuphilin-a in dense-core vesicle exocytosis. *Methods Enzymol.* **403**, 445-457.

Fukuda, M., Kanno, E. and Mikoshiba, K. (1999). Conserved N-terminal cysteine motif is essential for homo- and heterodimer formation of synaptotagmins III, V, VI, and X. *J. Biol. Chem.* **274**, 31421-31427.

Fukuda, M., Kuroda, T. S. and Mikoshiba, K. (2002). Slac2-a/melanophilin, the missing link between Rab27 and myosin Va: implications of a tripartite protein complex for melanosome transport. *J. Biol. Chem.* **277**, 12432-12436.

Fukuda, M., Kanno, E. and Yamamoto, A. (2004). Rabphilin and Noc2 are recruited to dense-core vesicles through specific interaction with Rab27A in PC12 cells. *J. Biol. Chem.* **279**, 13065-13075.

Fukuda, M., Kanno, E., Ishibashi, K. and Itoh, T. (2008). Large scale screening for novel rab effectors reveals unexpected broad Rab binding specificity. *Mol. Cell Proteomics* **7**, 1031-1042.

Hume, A. N., Collinson, L. M., Rapak, A., Gomes, A. Q., Hopkins, C. R. and

Seabra, M. C. (2001). Rab27a regulates the peripheral distribution of melanosomes in melanocytes. *J. Cell Biol.* **152**, 795-808.

Johansson, M., Rocha, N., Zwart, W., Jordens, I., Janssen, L., Kuijl, C., Olkkonen, V. M. and Neefjes, J. (2007). Activation of endosomal dynein motors by stepwise assembly of Rab7-RILP-p150^{Glued}, ORP1L, and the receptor βIII spectrin. *J. Cell Biol.* **176**, 459-471.

Jordens, I., Fernandez-Borja, M., Marsman, M., Dusseljee, S., Janssen, L., Calafat, J., Janssen, H., Wubbolts, R. and Neefjes, J. (2001). The Rab7 effector protein RILP controls lysosomal transport by inducing the recruitment of dynein-dynactin motors. *Curr. Biol.* **11**, 1680-1685.

Jordens, I., Westbroek, W., Marsman, M., Rocha, N., Mommaas, M., Huizing, M., Lambert, J., Naeyaert, J. M. and Neefjes, J. (2006). Rab7 and Rab27a control two motor protein activities involved in melanosomal transport. *Pigment Cell Melanoma Res.* **19**, 412-423.

Kuroda, T. S. and Fukuda, M. (2004). Rab27A-binding protein Slp2-a is required for peripheral melanosome distribution and elongated cell shape in melanocytes. *Nat. Cell Biol.* **6**, 1195-1203.

Kuroda, T. S. and Fukuda, M. (2005). Identification and biochemical analysis of Slac2-c/MyRIP as a Rab27A-, myosin Va/VIIa-, and actin-binding protein. *Methods Enzymol.* **403**, 431-444.

Kuroda, T. S., Ariga, H. and Fukuda, M. (2003). The actin-binding domain of

Slac2-a/melanophilin is required for melanosome distribution in melanocytes. *Mol. Cell Biol.* **23**, 5245-5255.

Kuroda, T. S., Fukuda, M., Ariga, H. and Mikoshiba, K. (2002). The Slp homology domain of synaptotagmin-like proteins 1-4 and Slac2 functions as a novel Rab27A binding domain. *J. Biol. Chem.* **277**, 9212-9218.

Marks, M. S. and Seabra, M. C. (2001). The melanosome: membrane dynamics in black and white. *Nat. Rev. Mol. Cell Biol.* **2**, 738-748.

Moore, K. J., Swing, D. A., Rinchik, E. M., Mucenski, M. L., Buchberg, A. M., Copeland, N. G. and Jenkins, N. A. (1988). The murine dilute suppressor gene *dsu* suppresses the coat-color phenotype of three pigment mutations that alter melanocyte morphology, *d, ash* and *ln*. *Genetics* **119**, 933-941.

O'Sullivan, T. N., Wu, X. S., Rachel, R. A., Huang, J. D., Swing, D. A., Matesic, L. E., Hammer, J. A., III, Copeland, N. G. and Jenkins, N. A. (2004). *dsu* functions in a MYO5A-independent pathway to suppress the coat color of *dilute* mice. *Proc. Natl. Acad. Sci. USA* **101**, 16831-16836.

Provance, D. W., James, T. L. and Mercer, J. A. (2002). Melanophilin, the product of the *leaden* locus, is required for targeting of myosin-Va to melanosomes. *Traffic* **3**, 124-132.

Raposo, G. and Marks, M. S. (2007). Melanosomes--dark organelles enlighten endosomal membrane transport. *Nat. Rev. Mol. Cell Biol.* **8**, 786-797.

Saegusa, C., Tanaka, T., Tani, S., Itohara, S., Mikoshiba, K. and Fukuda, M.

(2006). Decreased basal mucus secretion by Slp2-a-deficient gastric surface mucous cells. *Genes Cells* **11**, 623-631.

Seabra, M. C. and Coudrier, E. (2004). Rab GTPases and myosin motors in organelle motility. *Traffic* **5**, 393-399.

Strom, M., Hume, A. N., Tarafder, A. K., Barkagianni, E. and Seabra, M. C. (2002). A family of Rab27-binding proteins. Melanophilin links Rab27a and myosin Va function in melanosome transport. *J. Biol. Chem.* **277**, 25423-25430.

Sweet, H. O. (1983). Dilute suppressor, a new suppressor gene in the house mouse. *J. Hered.* **74**, 305-306.

Tamura, K., Ohbayashi, N., Ishibashi, K. and Fukuda, M. (2011). Structure-function analysis of VPS9-ankyrin-repeat protein (Varp) in the trafficking of tyrosinase-related protein 1 in melanocytes. *J. Biol. Chem.* **286**, 7507-7521.

Tsuboi, T. and Fukuda, M. (2006). Rab3A and Rab27A cooperatively regulate the docking step of dense-core vesicle exocytosis in PC12 cells. *J. Cell Sci.* **119**, 2196-2203.

Van Gele, M., Dynoodt, P. and Lambert, J. (2009). Griscelli syndrome: a model system to study vesicular trafficking. *Pigment Cell Melanoma Res.* **22**, 268-282.

Wang, T., Wong, K. K. and Hong, W. (2004). A unique region of RILP distinguishes it from its related proteins in its regulation of lysosomal morphology and interaction with Rab7 and Rab34. *Mol. Biol. Cell* **15**, 815-826.

Wu, M., Wang, T., Loh, E., Hong, W. and Song, H. (2005). Structural basis for

recruitment of RILP by small GTPase Rab7. *EMBO J.* **24**, 1491-1501.

Wu, X., Bowers, B., Rao, K., Wei, Q. and Hammer, J. A., III. (1998). Visualization of melanosome dynamics within wild-type and dilute melanocytes suggests a paradigm for myosin V function in vivo. *J. Cell Biol.* **143**, 1899-1918.

Wu, X. S., Rao, K., Zhang, H., Wang, F., Sellers, J. R., Matesic, L. E., Copeland, N. G., Jenkins, N. A. and Hammer, J. A., III. (2002). Identification of an organelle receptor for myosin-Va. *Nat. Cell Biol* **4**, 271-278.

Figure legends

Fig. 1. Knockdown of Mreg restores peripheral dispersion of melanosomes in melan-ash cells. (A) Expression of EGFP-Mreg (right), but not EGFP alone (left), induced perinuclear melanosome aggregation in melan-a cells. Note that Mreg strongly colocalized with melanosomes (arrows; melanosomes are pseudo-colored in red in the upper insets of the top panels, and the corresponding bright-field images are shown in the lower insets of the top panels). Bright-field images show the melanosome distribution in the cells (top). EGFP-expressing cells are outlined with a broken red line. The insets show magnified views of the boxed areas. (B) Knockdown of Mreg with specific shRNA had no effect on the peripheral melanosome distribution in melan-a cells. Melan-a cells were transfected with pSilencer-Mreg-st1/st2 (*Mreg* shRNA #1/#2) together with pEGFP-C1, and Mreg-deficient cells were identified by GFP fluorescence (bottom panels). (C) Knockdown of Mreg in melan-ash cells with specific shRNAs (or expression of EGFP-Rab27A) caused dispersion of melanosomes from around the nucleus to the cell periphery. Note that the melanosomes in the Mreg-deficient melan-ash cells were not observed just beneath the plasma membrane, in contrast to the EGFP-Rab27A-re-expressing melan-ash cells (i.e., rescue). Since the peripheral dispersion phenotype induced by *Mreg* shRNA #1 in melan-ash cells was completely restored by the co-expression of siRNA-resistant Mreg (see Supplemental Fig. S1), the observed effect must not have been caused by an off-target effect of shRNA. Scale bars, 10 μm. (D) RNAi-mediated knockdown of *Mreg* in melan-a cells (a) and melan-ash

cells (b) as revealed by an RT-PCR analysis. *G3PDH* expression (bottom panels) is shown as a reference to ensure that equivalent amounts of first strand cDNA were used for the RT-PCR analysis. The size of the molecular weight markers (bp, base pair) is shown on the left side of the panel. (E, F) The number of melanocytes showing perinuclear melanosome aggregation is expressed as a percentage of the number of melanocytes bearing EGFP fluorescence shown in (A, B). (G) The number of melanocytes showing peripheral dispersion is expressed as a percentage of the number of melanocytes bearing EGFP fluorescence shown in (C). *, p <0.01 in comparison with the control (Student's unpaired *t* test).

Fig. 2. Endogenous Mreg protein is localized on mature melanosomes. Immunoaffinity purification of Rab27A-bound melanosomes from B16-F1 cells with anti-Rab27A IgG-conjugated magnetic beads was performed as described previously (Kuroda and Fukuda, 2004). Melanosomal fractions were analyzed by 10% SDS-PAGE followed by immunoblotting with anti-Mreg antibody (0.6 μg/ml), anti-Rab27A antibody (1.6 μg/ml), anti-tyrosinase antibody (0.3 μg/ml), anti-Tyrp1 antibody (0.1 μg/ml), anti-Lamp1 antibody (1 μg/ml), anti-EEA1 antibody (1/1000 dilution), anti-TfR antibody (0.5 μg/ml), anti-GM130 antibody (0.3 μg/ml), anti-calreticulin antibody (1/1000 dilution), and anti-γ-adaptin antibody (0.25 μg/ml). The amount of IgG heavy chain (HC) used for immunoprecipitation was determined by amido black staining of the blots (bottom panel). Input means 1% volume of the crude membrane fractions used for immunoaffinity-purification (lane 1). Note that Mreg was co-purified with

melanosome markers (lane 3 in the top four panels), but not other organelle markers. The positions of the molecular mass markers ($\times 10^{-3}$) are shown on the left.

Fig. 3. Functional disruption of a dynein-dynactin motor complex restores peripheral dispersion of melanosomes in melan-ash cells. (A) Expression of $p50^{dynamitin}$ caused melanosomes to disperse from around the nucleus to the cell periphery. Melan-ash cells were transfected with a control pEGFP-C1 (left) or pEGFP-C1-$p50^{dynamitin}$ (right). (B) Knockdown of $p150^{Glued}$ with specific siRNAs caused melanosomes to disperse from around the nucleus to the cell periphery. Melan-ash cells were transfected with a control siRNA or *p150*^{Glued} siRNAs and immunostained with anti-$p150^{Glued}$ antibody (bottom). Bright-field images show the melanosome distribution in the cells (top). EGFP (or siRNA)-expressing cells are outlined with a broken red line. (C) Co-expression of $p50^{dynamitin}$ with Mreg restored the peripheral melanosome distribution of melan-a cells. Melan-a cells were transfected with a control pEF-T7-GST vector (left) or pEF-T7-$p50^{dynamitin}$ (right) together with pEF-FLAG-Mreg. Bright-field images show the melanosome distribution in the cells (bottom). Scale bars, 10 μm. (D, E) The number of melanocytes showing peripheral dispersion is expressed as a percentage of the number of melanocytes bearing EGFP fluorescence shown in (A, B). (F) The number of melanocytes showing perinuclear melanosome aggregation is expressed as a percentage of the number of melanocytes expressing FLAG-Mreg shown in (C). *, p <0.01 in comparison with the control (Student's unpaired t test). (G) Efficiency of siRNAs targeted against $p150^{Glued}$. The

siRNAs against p150^{Glued} were transfected into melan-a cells, and their cell lysates were subjected to 10% SDS-PAGE followed by immunoblotting with anti-p150^{Glued} antibody (1/4000 dilution) and anti-actin antibody (1/10,000 dilution). The positions of the molecular mass markers ($\times 10^{-3}$) are shown on the left.

Fig. 4. Mreg interacts with RILP. (A) Schematic representation of the mouse RILP and RILP-L1. The two coiled-coil (CC) domains (named CC1 and CC2) are indicated by shaded boxes. The degree of amino acid identity in the CC domains of RILP and RILP-L1 is indicated by percentages. (B) Interaction between Mreg and RILP as revealed by a co-immunoprecipitation assay in COS-7 cells. Beads coupled with either FLAG-Rab27A (lanes 1 and 2), FLAG-Rab7 (lanes 3 and 4), FLAG-Rab34 (lanes 5 and 6), and FLAG-Mreg (lanes 7 and 8) were incubated with COS-7 cell lysates containing T7-RILP (lanes 1, 3, 5, and 7) or T7-RILP-L1 (lanes 2, 4, 6, and 8), and the proteins bound to the beads were analyzed by immunoblotting with indicated antibodies. Note that both RILP and RILP-L1 interacted with Rab34 (lanes 5 and 6 in the middle panel) but that only RILP interacted with Rab7 and Mreg (lanes 3 and 7 in the middle panel). (C) Knockdown of RILP, but not of RILP-L1, with specific shRNAs caused melanosomes to disperse from around the nucleus to the cell periphery. Melan-ash cells were transfected with a control vector, *RILP* shRNA expression vectors, or *RILP-L1* shRNA expression vectors together with the EGFP expression vector as a transfection marker. Bright-field images show the melanosome distribution in the cells. EGFP-expressing cells are outlined with a broken red line. Since the peripheral

dispersion phenotype induced by *RILP* shRNA #1 in melan-ash cells was completely restored by the co-expression of siRNA-resistant RILP (see Supplemental Fig. S2), the observed effect must not have been caused by an off-target effect of shRNA. Scale bars, 10 μm. (D) The number of melanocytes showing peripheral dispersion is expressed as a percentage of the number of melanocytes bearing EGFP fluorescence shown in (C). *, $p < 0.01$ in comparison with the control (Student's unpaired *t* test). (E) RNAi-mediated knockdown of *RILP* (a) and *RILP-L1* (b) in melan-ash cells as revealed by an RT-PCR analysis. *G3PDH* expression (bottom panels) is shown as a reference to ensure that equivalent amounts of first strand cDNA were used for the RT-PCR analysis. The size of the molecular weight markers (bp, base pair) is shown on the left side of the panel. (F) Mapping of the site responsible for Mreg-binding in RILP. The truncated mutants of RILP used in this study (RILP-N and RILP-C) are shown at the top. Glutathione-Sepharose beads coupled with nothing, T7-GST-RILP-N, or T7-GST-RILP-C were incubated with solutions containing HA-Mreg, and the proteins bound to the beads were analyzed by immunoblotting with indicated antibodies. (G) Competition experiments revealed that Mreg-binding and Rab7-binding of RILP are mutually exclusive. Glutathione-Sepharose beads coupled with T7-GST-RILP-C or beads alone were incubated with solutions containing T7-Mreg and/or increasing amount of FLAG-Rab7, and the proteins bound to the beads were analyzed by immunoblotting with indicated antibodies. Input means 1/80 volume (in B, F) or 1/100 volume (in G), of the reaction mixture used for immunoprecipitation. The positions of the molecular mass markers ($\times 10^{-3}$) are shown on the left.

Fig. 5. Mapping of the sites responsible for RILP binding and melanosomal localization of Mreg, and its interaction with RILP·p150^{Glued}. (A) Schematic representation of the mouse Mreg and its truncated mutants (named Mreg-ΔN and Mreg-ΔC) used in this study. (B) Interaction between RILP and the C-terminal portion of Mreg as revealed by a co-immunoprecipitation assay in COS-7 cells. Beads coupled with nothing (lane 1), FLAG-Mreg (lane 2), FLAG-Mreg-ΔN (lane 3), or FLAG-Mreg-ΔC (lane 4), were incubated with COS-7 cell lysates containing T7-GST-RILP, and the proteins bound to the beads were analyzed by 10% SDS-PAGE followed by immunoblotting with HRP-conjugated anti-T7 tag antibody (top panel) and HRP-conjugated anti-FLAG tag antibody (bottom panel). Input means 1/80 volume of the reaction mixture used for immunoprecipitation (middle panel). Note that the C-terminal portion of Mreg (140-214) is necessary for RILP binding. (C) The N-terminal portion of Mreg is required for melanosomal localization in melan-a cells. Melan-a cells were transfected with pEGFP-C1-Mreg (top panels), pEGFP-C1-Mreg-ΔN (middle panels), or pEGFP-C1-Mreg-ΔC (bottom panels). Bright-field images show the melanosome distribution in the cells (right panels). The insets show magnified views of the boxed areas (melanosomes are pseudo-colored in red in the upper inset of the right panels). Note that both Mreg and Mreg-ΔC, but not Mreg-ΔN, colocalized with mature melanosomes. Scale bars, 10 μm. (D) *In vitro* formation of the Mreg·RILP·p150^{Glued} complex from purified components. Beads coupled with FLAG-p150^{Glued} were incubated with purified GST-Mreg in the absence or

presence of T7-GST-RILP, and the proteins bound to the beads were analyzed by immunoblotting with the antibodies indicated. (E) Formation of the Mreg·RILP·p150^{Glued} complex in B16-F1 cells. Endogenous Mreg molecules were immunoprecipitated from lysates of B16-F1 cells expressing control shRNA (lanes 1 and 4) or *RILP* shRNA #1/#2 (lanes 2, 3, 5, and 6) with anti-Mreg specific IgG (lanes 4-6) or control IgG (lanes 1-3). Mreg, RILP, and p150^{Glued} were analyzed by immunoblotting with specific antibodies. It should be noted that the amount of co-immunoprecipitated p150^{Glued} with Mreg was clearly reduced in RILP-knockdown cells (second panel). Because of the presence of IgG heavy chain, co-immunoprecipitated RILP was unable to be detected under our experimental conditions (data not shown). However, when FLAG-RILP was expressed in melanocytes, the co-immunoprecipitation of FLAG-RILP with endogenous Mreg and p150^{Glued} was evident (see Supplemental Fig. S4), indicating that the Mreg-RILP interaction likely occurs in cultured melanocytes. Input means 1/100 volume (in D, E), of the reaction mixture used for immunoprecipitation (IP). The positions of the molecular mass markers ($\times 10^{-3}$) are shown on the left.

Fig. 6. Effect of expression of the C-terminal domain of RILP on melanosome distribution in melanocytes. (A) Expression of RILP-C in melan-ash cells restored the peripheral dispersion of melanosomes. Melan-ash cells were transfected with a control pmStr-C1 vector (top panels), pmStr-C1-RILP-N (middle panels), or pmStr-C1-RILP-C (bottom panels). Bright-field images show the melanosome distribution in the cells

(right panels). The insets show magnified views of the boxed areas (melanosomes are pseudo-colored in green). mStr-expressing cells are outlined with a broken red line. Note that mStr-RILP-C often colocalized with mature melanosomes (arrows in the upper inset of the bottom right panel; corresponding bright-field image is shown in the lower inset), whereas no melanosomal localization of mStr-RILP-N was observed (red and green signals were clearly separate). Scale bars, 10 μm. (B) The number of melanocytes showing peripheral dispersion is expressed as a percentage of the number of melanocytes bearing mStr fluorescence shown in (A). *, $p < 0.01$ in comparison with the control (Student's unpaired *t* test). The data shown are means and SD of data from three independent experiments ($n > 50$). (C) Expression of the C-terminal domain of RILP (RILP-C) in melan-a cells attenuated the perinuclear melanosome aggregation phenotype induced by Mreg expression. Melan-a cells were transfected with a control pmStr-C1 vector (left panels), pmStr-C1-RILP-full (left middle panels), pmStr-C1-RILP-N (right middle panels), or pmStr-C1-RILP-C (right panels) together with pEGFP-C1-Mreg. Bright-field images show the melanosome distribution in the cells (bottom panels). The insets show magnified views of the boxed areas (melanosomes are pseudo-colored in blue). pmStr-expressing cells are outlined with a broken red line. Note that mStr-RILP-C often colocalized with mature melanosomes together with Mreg (arrows and arrowheads in the insets) and clearly attenuated the perinuclear aggregation phenotype induced by expression of Mreg. Scale bars, 10 μm. (D) The number of melanocytes showing perinuclear aggregation is expressed as a percentage of the number of melanocytes bearing mStr fluorescence shown in (C)

(co-expression of EGFP-Mreg and mStr-RILP mutants: right four columns) and Fig. S5 (expression of mStr-RILP mutants alone: left four columns). *, p <0.01 in comparison with the mStr-expressing cells or mStr/EGFP-Mreg-expressing cells (Student's unpaired *t* test). The data shown are means and SD of data from three independent experiments (n >50).

Fig. S1. Re-expression of siRNA-resistant Mreg^{SR} in Mreg-deficient melan-ash cells restored the perinuclear aggregation phenotype. (A) Rab27A-defective melan-ash cells were co-transfected with pSilencer-Mreg-st1 (*Mreg* shRNA #1) and pEGFP-C1 or pEGFP-C1-Mreg^{SR}. Note that the dispersion of melanosomes was evident in the Mreg-deficient melan-ash cells (left panels), whereas the re-expression of Mreg^{SR} restored the perinuclear aggregation phenotype of melanosomes. Bright-field images show the melanosome distribution in the cells (top). EGFP-expressing cells are outlined with a broken red line. The insets show magnified views of the boxed areas (melanosomes are pseudo-colored in red). Scale bars, 10 μm. (B) The number of melanocytes showing peripheral melanosome dispersion is expressed as a percentage of the number of melanocytes bearing EGFP fluorescence shown in (A). ∗, p <0.01 in comparison with the control (Student's unpaired t test). (C) An siRNA-resistant (SR) mutant of Mreg. pEGFP-C1-Mreg (lanes 1 and 2) or pEGFP-C1-Mreg^{SR} (lanes 3 and 4) was co-transfected into COS-7 cells together with pSilencer-Mreg-st1 or a control vector. Cell lysates were subjected to 10% SDS-PAGE followed by immunoblotting with anti-GFP antibody (1/3000 dilution; top panel) and anti-actin antibody (1/10,000 dilution; bottom panel). The positions of the molecular mass markers ($\times 10^{-3}$) are shown on the left.

Fig. S2. Re-expression of siRNA-resistant RILP^{SR} in RILP-deficient melan-ash cells restored the perinuclear aggregation phenotype. (A) Rab27A-defective melan-ash cells were co-transfected with pSilencer-RILP-st1 (*RILP* shRNA #1) and

pEGFP-C1 or pEGFP-C1-RILP^{SR}. Note that the dispersion of melanosomes was evident in the RILP-deficient melan-ash cells (left panels), whereas the re-expression of RILP^{SR} restored the perinuclear aggregation phenotype of melanosomes. Bright-field images show the melanosome distribution in the cells (top). EGFP-expressing cells are outlined with a broken red line. Scale bars, 10 μm. (B) The number of melanocytes showing peripheral melanosome dispersion is expressed as a percentage of the number of melanocytes bearing EGFP fluorescence shown in (A). ∗, p <0.01 in comparison with the control (Student's unpaired t test). (C) An siRNA-resistant (SR) mutant of RILP. pEGFP-C1-RILP (lanes 1 and 2) or pEGFP-C1-RILP^{SR} (lanes 3 and 4) was co-transfected into COS-7 cells together with pSilencer-RILP-st1 or a control vector. Cell lysates were subjected to 10% SDS-PAGE followed by immunoblotting with anti-GFP antibody (1/3000 dilution; top panel) and anti-actin antibody (1/10,000 dilution; bottom panel). The positions of the molecular mass markers ($\times 10^{-3}$) are shown on the left. (D) The knockdown of RILP with specific shRNA had no effect on the melanosome distribution in melan-a cells. Melan-a cells were transfected with a control vector or the *RILP* shRNA #1 expression vector together with the EGFP expression vector as a transfection marker. Bright-field images (top panels) show the melanosome distribution in the cells. Scale bars, 10 μm.

Fig. S3. Expression of Rab7 and knockdown of Rab7 with specific shRNA had no effect on melanosome distribution in melan-a cells and melan-ash cells, respectively. (A) Melan-a cells expressing EGFP alone (control; left panels), EGFP-Rab7 (middle

panels), or EGFP-Rab7(Q67L) (right panels) are shown. The insets show magnified views of the boxed areas (melanosomes are pseudo-colored in red). (B) Melan-ash cells transfected with a control vector or *Rab7* shRNA (#1) expression vector together with the EGFP expression vector as a transfection marker (bottom panels) are shown. Bright-field images show the melanosome distribution in the cells (top panels). EGFP-expressing cells are outlined with a broken red line. Scale bars, 10 μm. (C) The number of melanocytes showing peripheral dispersion is expressed as a percentage of the number of melanocytes bearing EGFP fluorescence shown in (B). (D) The RNAi-mediated knockdown of Rab7 in melan-ash cells caused an increase in the amount of EGFR. Lysates of cells treated with control or *Rab7* siRNA were analyzed by immunoblotting with the antibodies indicated. The positions of the molecular mass markers ($\times 10^{-3}$) are shown on the left.

Fig. S4. Formation of the Mreg·FLAG-RILP·p150^{Glued} complex in B16-F1 cells. FLAG-RILP was transiently expressed in B16-F1 cells and the Mreg·FLAG-RILP·p150^{Glued} complex was immunoprecipitated using anti-Mreg-specific antibody as described under Materials and Methods. Note that both FLAG-RILP and p150^{Glued} were co-purified with Mreg (lane 2). Input means 1/100 volume of the reaction mixture used for immunoprecipitation (IP). The positions of the molecular mass markers ($\times 10^{-3}$) are shown on the left.

Fig. S5. Expression of RILP, but not of its truncated mutants, in melan-a cells

induced perinuclear aggregation of melanosomes. Melan-a cells were transfected with a control pmStr-C1 vector (top panels), pmStr-C1-RILP-full (second panels), pmStr-C1-RILP-N (third panels), or pmStr-C1-RILP-C (bottom panels). Bright-field images show the melanosome distribution in the cells (right panels). The insets show magnified views of the boxed areas (melanosomes are pseudo-colored in green in the upper insets of the bright-filed images). An mStr-expressing cell is outlined with a broken line. Note that approximately 40% of the cells expressing full-length mStr-RILP showed the perinuclear aggregation phenotype and that the same phenotype was further manifested by the co-expression of mStr-RILP with EGFP-Mreg (see Fig. 6D). Arrows in the upper insets show the colocalization of RILP (or RILP-C) with mature melanosomes (corresponding bright-field images are shown in the lower insets). Scale bars, 10 μm.

Fig. S6. Knockdown of Mreg, RILP, and p150^{Glued} in cytochalasin D-treated melan-a cells with specific shRNA/siRNA caused the dispersion of melanosomes from around the nucleus to the cell periphery. (A) Melan-a cells were transfected with a control pEGFP-C1 vector (a), pSilencer-Mreg-st1 (*Mreg* shRNA #1) (b), pSilencer-RILP-st1 (*RILP* shRNA #1) (c), or *p150^{Glued}* siRNA #1 (d). At 48 hours after transfection, the melan-a cells were treated with DMSO or cytochalasin D (0.5 μM) for 1 hour. Bright-field images show the melanosome distribution in the cells. Cytochalasin D-treated EGFP-expressing cells is outlined with a broken red line. Scale bars, 20 μm. (B) The number of melanocytes showing perinuclear melanosome aggregation is

expressed as a percentage of the number of melanocytes expressing EGFP shown in (A). ∗, p <0.01 in comparison with the control (Student's unpaired t test). Note that cytochalasin D treatment induced the perinuclear aggregation of melanosomes in melan-a cells, whereas the knockdown of either Mreg, RILP, or $p150^{Glued}$, restored the peripheral melanosome distribution.

Fig. S7. Schematic model of the retrograde melanosome transport complex composed of Mreg, RILP, $p150^{Glued}$, and dynein. Mreg is present on mature melanosomes (Figs. 1 and 2). RILP is first recruited to Mreg-bound melanosomes through the direct interaction of Mreg with the C-terminal domain of RILP (Fig. 4F) and then recruits the dynein-dynactin motor through the interaction of $p150^{Glued}$ with the N-terminal domain of RILP (Fig. 5D). The resulting protein complex regulates microtubule-dependent retrograde melanosome transport in melanocytes.

Fig. S8. (for reviewers only) Expression of Rab7-Q67L and knockdown of Rab7 with specific shRNA had no effect on Pmel17 distribution in melan-a cells. (A) Melan-a cells expressing EGFP alone (control; top left panels) or EGFP-Rab7(Q67L) (top right panels) were immunostained with anti-Pmel17 antibody (bottom panels). (B) Melan-a cells transfected with a control vector or *Rab7* shRNA (#1) expression vector together with the EGFP expression vector as a transfection marker (top panels) were immunostained with anti-Pmel17 antibody. Bright-field images show the melanosome distribution in the cells (bottom panels). Note that the Pmel17 distribution

was unaffected by either the expression of Rab7-Q67L or the knockdown of endogenous Rab7 in melan-ash cells, unlike the results of a previous report (Jordens et al., 2006). EGFP-expressing cells are outlined with a broken ine. Scale bars, 10 μm.

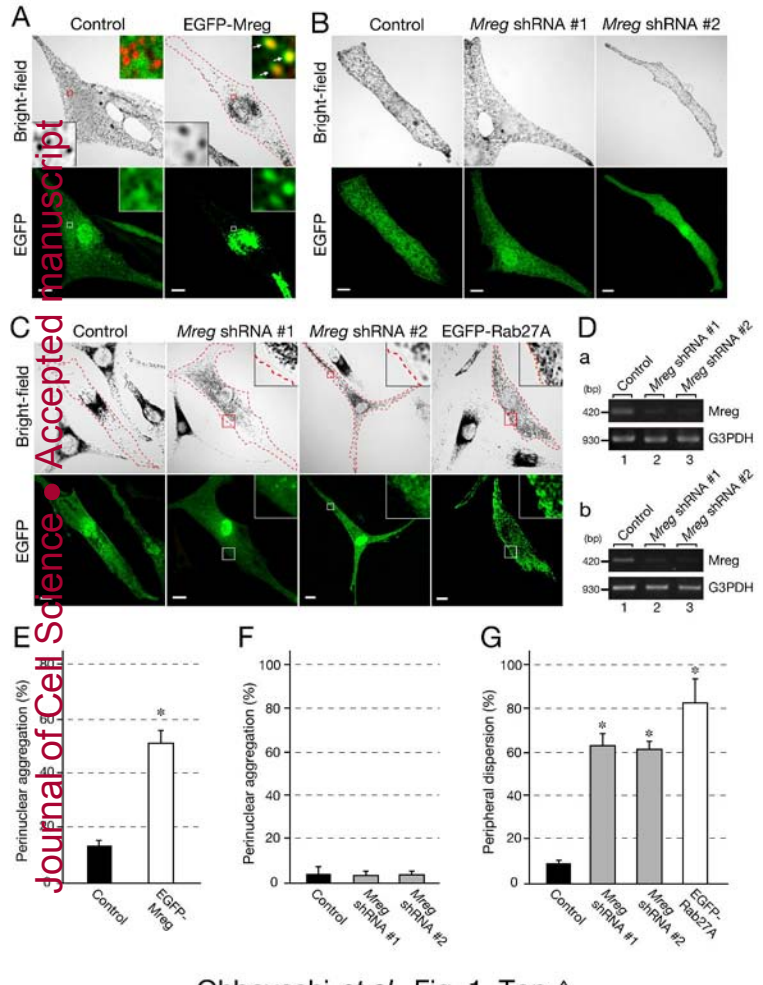

Ohbayashi *et al.*, Fig. 1, Top ⇑

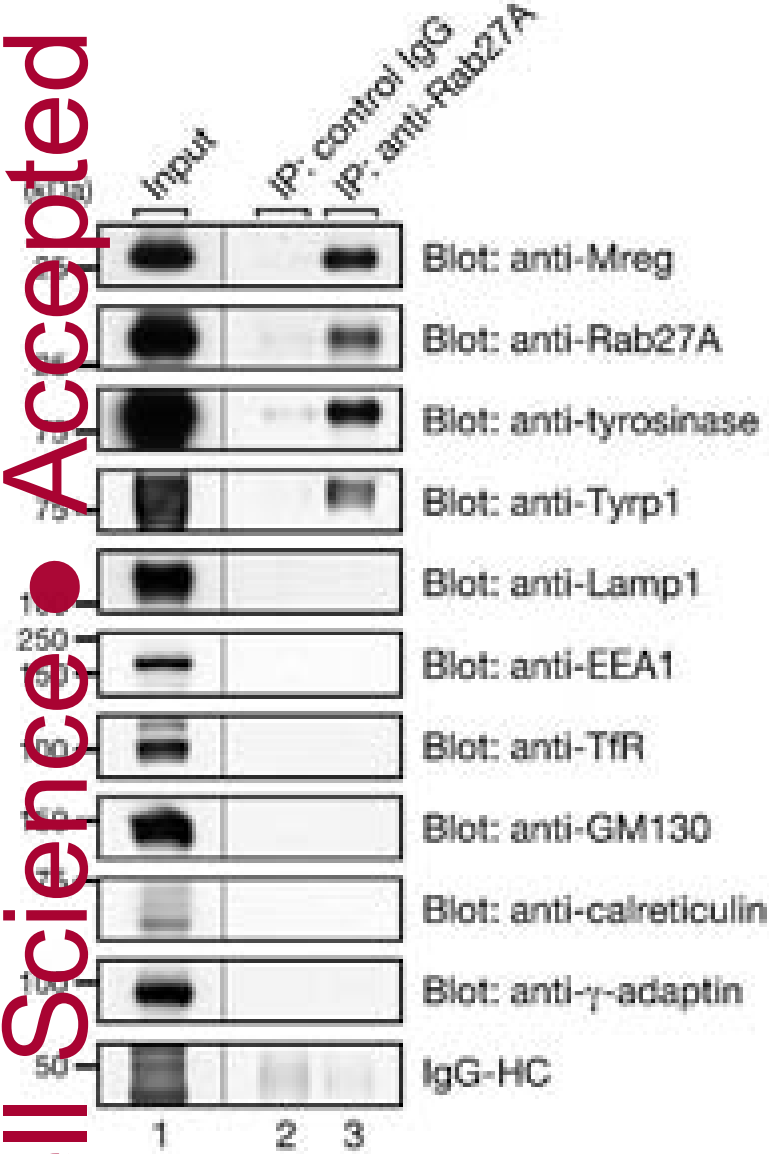

Ohbayashi *et al.*, Fig. 2, Top ⇑

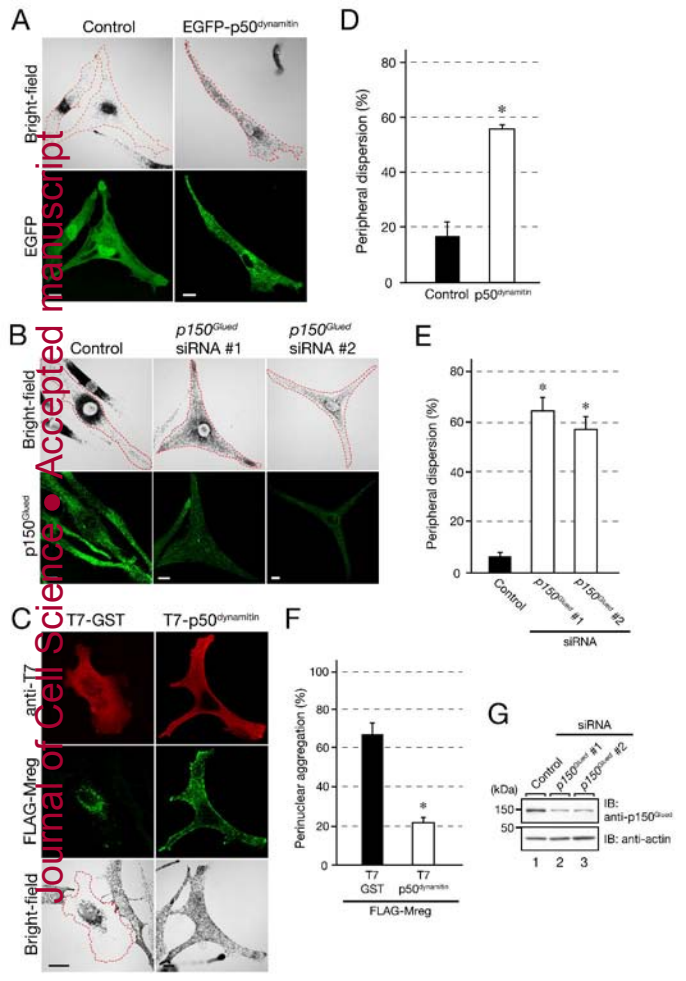

Ohbayashi *et al.*, Fig. 3, Top ⇑

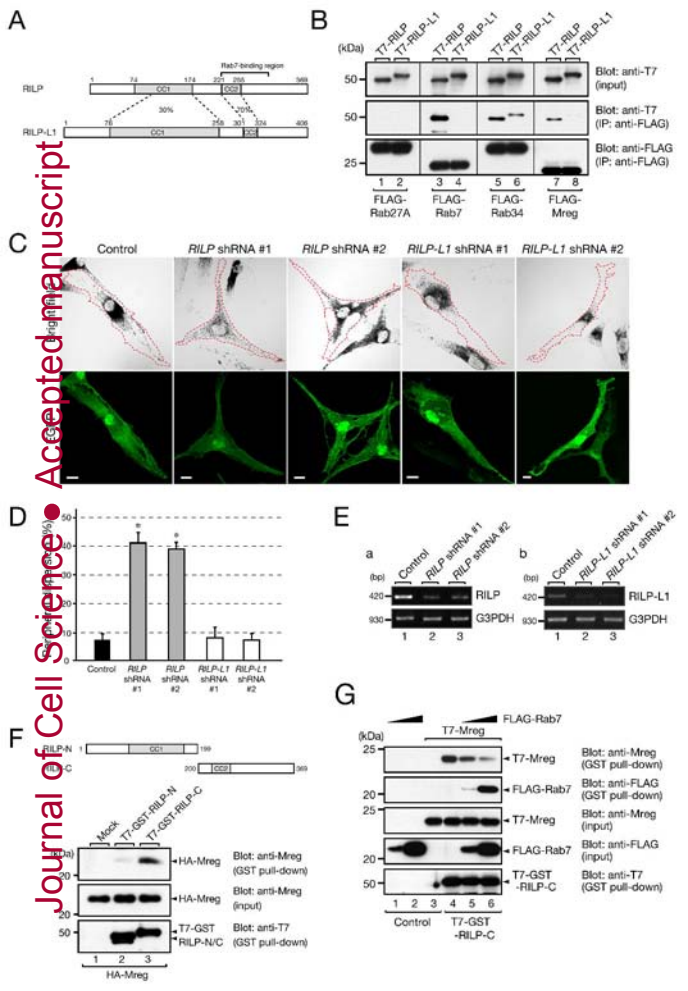

Ohbayashi *et al.*, Fig. 4, Top ⇑

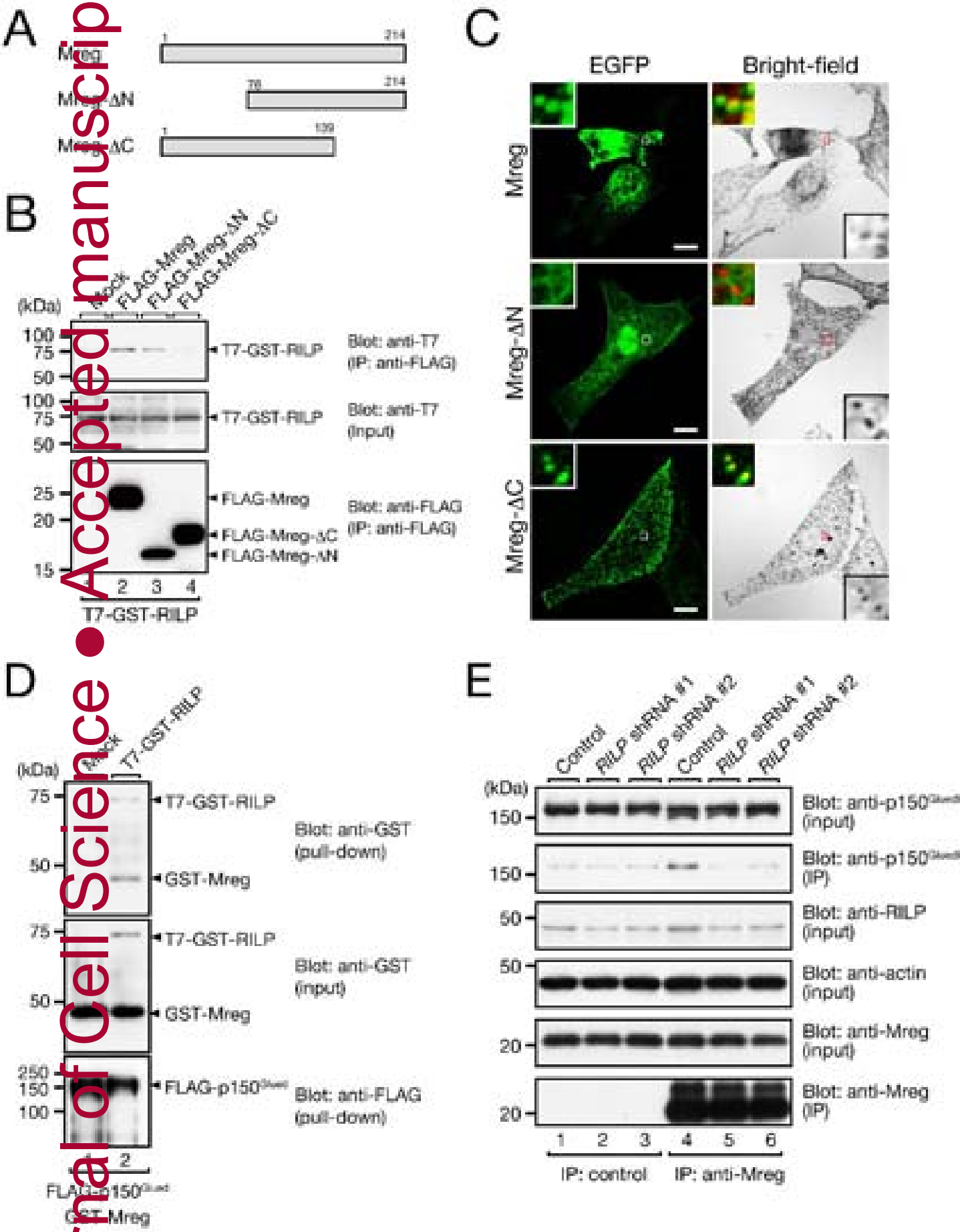

Ohbayashi *et al.*, Fig. 5, Top ⇑

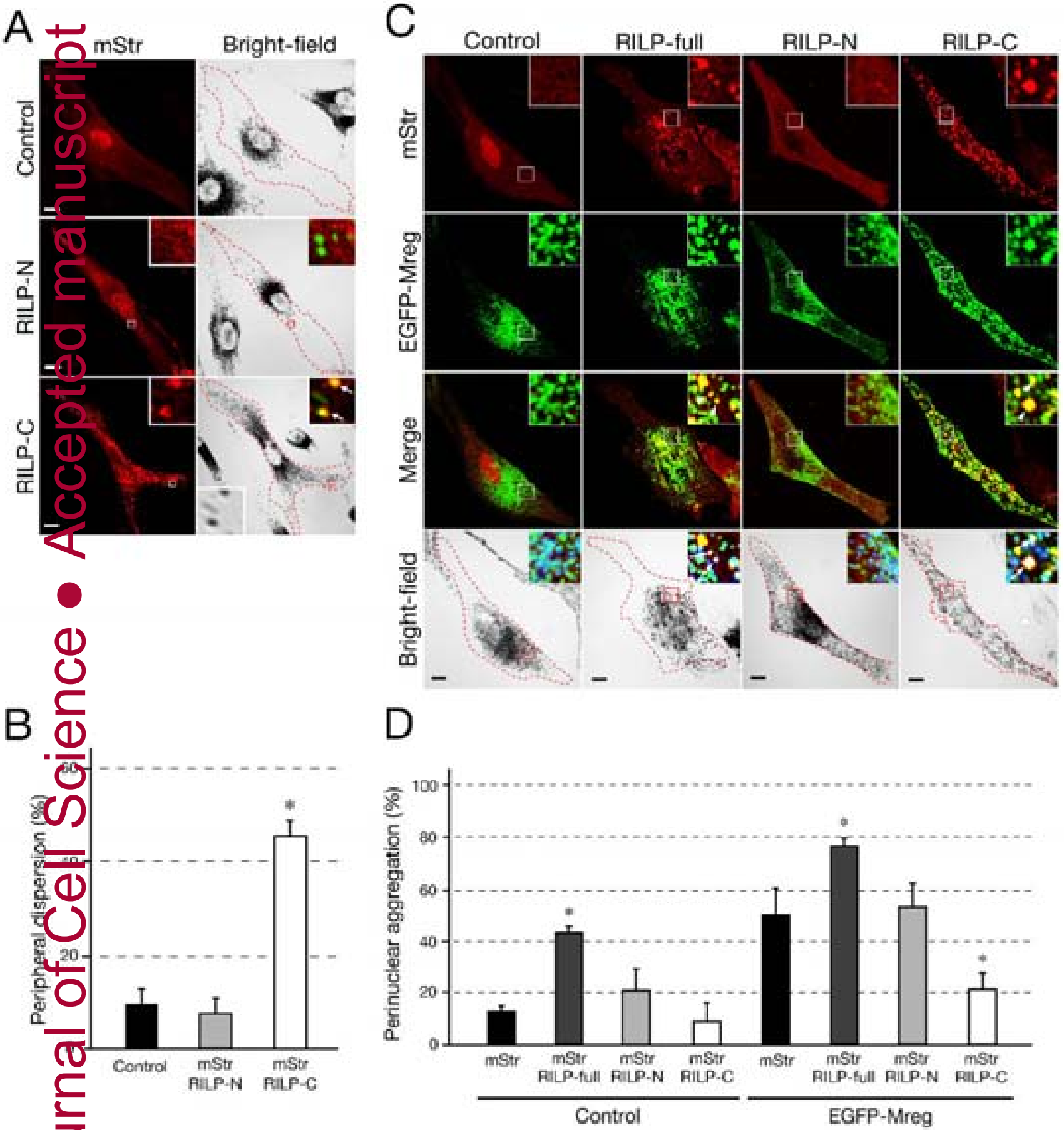

Ohbayashi *et al.*, Fig. 6, Top ⇑